832 *Chem. Mater.* **2010,** *22,* 832–839
DOI:10.1021/cm901542w

CHEMISTRY OF MATERIALS
Article

Pt Nanoparticles Supported on Nitrogen-Doped Porous Carbon Nanospheres as an Electrocatalyst for Fuel Cells†

Fabing Su,*,‡,§ Zhiqun Tian,‡ Chee Kok Poh,‡ Zhan Wang,‡ San Hua Lim,‡ Zhaolin Liu,*,∥ and Jianyi Lin*,‡

‡*Institute of Chemical Engineering and Sciences, 1 Pesek Road, Jurong Island, Singapore 627833,* §*State Key Laboratory of Multi-phase Complex System, Institute of Process Engineering, Chinese Academy of Sciences, Beijing, China 100190, and* ∥*Institute of Materials Research and Engineering of Singapore, 3 Research Link, Singapore 117602*

Received June 5, 2009. Revised Manuscript Received September 9, 2009

Nitrogen-doped porous carbon nanospheres (PCNs) with a high surface area were prepared by chemical activation of nonporous carbon nanospheres (CNs). CNs were obtained via carbonization of polypyrrole nanospheres (PNs) that were synthesized by ultrasonic polymerization of pyrrole. The catalysts Pt/PCN, Pt/CN, and Pt/PN were prepared by depositing Pt nanoparticles on supports PCNs, CNs, and PNs, respectively, using ethylene glycol chemical reduction. Nitrogen adsorption, X-ray diffraction, thermogravimetric analysis, transmission electron microscopy, scanning electron microscopy, and X-ray photoelectron spectroscopy were employed to characterize samples. It was found that after chemical activation using KOH, PCNs containing N functional groups (mainly N-6 and N-Q) possessed a microporous structure with a high surface area of 1010 m^2/g and a particle size of less than 100 nm. The electrochemical properties of samples Pt/PCN, Pt/CN, and Pt/PN, together with commercial catalysts E-TEK (40 wt % Pt loading), were comparatively investigated in methanol oxidation reaction (MOR) and oxygen reduction reaction (ORR) for fuel cells. The results showed that the catalytic activity of Pt/PN toward both reactions at room temperature is almost negligible possibly due to the poor conductivity of support PNs proven by impedance spectroscopy, in contrast with some literature reports. Compared to Pt/CN and E-TEK catalyst, Pt/PCN revealed an enhanced mass activity in ORR and MOR because of the high dispersion of small Pt nanoparticles, the presence of nitrogen species, and developed microporous structure of support PCNs.

1. Introduction

Fuel cells as clean energy devices such as proton exchange membrane fuel cells (PEMFCs) and direct methanol fuel cells (DMFCs) have received substantial attention.[1] In these devices, Pt/carbon catalysts are generally used as electrode materials for chemical energy conversion of a fuel to electricity via electrocatalytic reactions, for example, methanol oxidation reaction (MOR) at the anodes of DMFCs and oxygen reduction reaction (ORR) at the cathodes of PEMFCs. To achieve high dispersion, utilization, activity, and stability of noble Pt,[2] carbon materials as supports with developed pore structure, high surface area, nanoscaled morphology, tunable surface chemistry, and good electric conductivity are highly desirable for electrocatalysts.[3,4]

It has been proven that the presence of functional groups such as N species on the carbon support surface could lead to the high dispersion of fine Pt nanoparticles with the synergistic interaction of Pt and support, resulting in the improved catalytic activity and durability toward ORR and MOR.[5] Carbon materials coated with N-containing polymers such as polypyrrole and polyaniline have been found to be the potential electrocatalyst supports, such as polypyrrole/carbon composites,[6,7] polypyrrole−carbon nanotubes,[8−10] polypyrrole−carbon black,[11,12] poly(vinylpyrrolidone)−modified graphite carbon nanofibers,[13] and polyaniline−carbon films.[14] However, polymer coating may cause some problems, for example, lowering the conductivity of carbon supports,[6] blocking the pore structure,[15]

† Accepted as part of the 2010 "Materials Chemistry of Energy Conversion Special Issue".

*To whom correspondence should be addressed. E-mail: fbsu@home.ipe.ac.cn (F.S.); Lin_Jianyi@ices.a-star.edu.sg (J.L.); zl-liu@imre.a-star.edu.sg (Z.L.).

(1) Winter, M.; Brodd, R. J. *Chem. Rev.* **2004**, *104*, 4245–4270.
(2) Gasteiger, H. A.; Markovi, X. M. N. *Science* **2009**, *324*, 48–49.
(3) Dicks, A. L. *J. Power Sources* **2006**, *156*, 128–141.
(4) McCreery, R. L. *Chem. Rev.* **2008**, *108*, 2646–2687.
(5) Shao, Y.; Sui, J.; Yin, G.; Gao, Y. *Appl. Catal., B* **2008**, *79*, 89–99.
(6) Zhao, H.; Li, L.; Yang, J.; Zhang, Y. *J. Power Sources* **2008**, *184*, 375–380.
(7) Choi, Y. S.; Joo, S. H.; Lee, S. A.; You, D. J.; Kim, H.; Pak, C.; Chang, H.; Seung, D. *Macromolecules* **2006**, *39*, 3275–3282.
(8) Selvaraj, V.; Alagar, M. *Electrochem. Commun.* **2007**, *9*, 1145–1153.
(9) Zhao, H.; Yang, J.; Li, L.; Li, H.; Wang, J.; Zhang, Y. *Int. J. Hydrogen Energy* **2009**, *34*, 3908–3914.
(10) Mohana Reddy, A. L.; Rajalakshmi, N.; Ramaprabhu, S. *Carbon* **2008**, *46*, 2–11.
(11) Zhao, H.; Li, L.; Yang, J.; Zhang, Y.; Li, H. *Electrochem. Commun.* **2008**, *10*, 876–879.
(12) Bashyam, R.; Zelenay, P. *Nature* **2006**, *443*, 63–66.
(13) Hsin, Y. L.; Hwang, K. C.; Yeh, C. T. *J. Am. Chem. Soc.* **2007**, *129*, 9999–10010.
(14) Wu, G.; Li, L.; Li, J.-H.; Xu, B.-Q. *Carbon* **2005**, *43*, 2579–2587.
(15) Wampler, W. A.; Wei, C.; Rajeshwar, K. *Chem. Mater.* **1995**, *7*, 585–592.

 Published on Web 09/30/2009

agglomerating the carbon particle,[6] and shortening the durability of supports due to the inherent instability of polymer in harsh operation circumstance,[6,16] which are not desired for electrocatalysts. Thus, much work focused on the N-doped carbon materials with N species incorporated in the carbon matrix to promote the Pt/carbon electrocatalyst performance. For example, Pt-based metal nanoparticles supported on carbon nitride (CNx) materials[16−20] and N-containing mesoporous carbons[21,22] exhibited high electrocatalytic activities in MOR and/or ORR. Nonprecious metal electrocatalysts supported on N-doped carbon materials[22−24] also showed a good performance for ORR. On the other hand, pore structure including mesopores and micropores in templated carbon supports has been demonstrated to play a significant role in transferring the mass products in MOR and ORR.[25,26] It should be mentioned that the commercial electrocatalyst supports such as carbon black XC-72 and BP2000 are carbon nanoparticles with a diameter of less than 100 nm. The voids among these nanoparticles could form a three-dimensional mesoporous structure that provides a rapid mass transport within electrodes. However, these particles do not contain N species. Recently, Lei et al.[27] and Choi et al.[28] have found that the N-doped carbon nanoparticles as Pt catalyst support was superior compared to XC-72 in MOR activity, but these carbon nanoparticles have no developed pore structure. Importantly, N-doped carbon materials have been demonstrated to serve as metal-free catalysts toward ORR,[29−33] and high surface area may offer more active sites.

Herein, we report the preparation and characterization of N-doped porous carbon nanospheres (PCNs), which possess distinguished advantages as an alternative electrocatalyst support. PCNs were obtained by chemical activation of nonporous carbon nanospheres (CNs) that were prepared by carbonizing polypyrrole nanospheres (PNs) at high temperature. The electrocatalytic properties of electrocatalysts Pt/PCN, Pt/CN, and Pt/PN were comparatively examined for MOR and ORR. It was found that toward MOR and ORR, polymer-supported Pt/PN catalyst is almost inactive against the previous results reported,[16,34] and Pt/PCN showed a better performance than Pt/CN and commercial E-TEK catalyst (40 wt % of Pt), indicating a highly potential application of PCNs in fuel cells.

2. Experimental Section

2.1. Synthesis of Support Nanospheres and Pt Catalysts. The sample PNs and CNs were prepared using a method previously reported.[35] In a typical synthesis, a mixture containing decyl alcohol (1-decanol, 99%, Aldrich) (1.0 g) and deionized water (30 mL) was stirred at 1 °C for 10 min. Then, dodecyltrimethylammonium bromide (DTAB, 99%, Aldrich) (1.5 g) was added to this mixture still under stirring at 1 °C for 20 min. The above mixture was transferred into a plastic tube. Subsequently, a 0.8 g of pyrrole (98%, Aldrich) was added dropwise into the tube, which was sonicated in an ultrasonicator (Elma Transsonic T460/H of capacity 2.75 L and frequency of 35 kHz). After 2 min, powdered $FeCl_3$ (99%, Aldrich) (2.0 g) was added into the tube. After further ultrasonication for 20 min, the product PNs were separated by filtration, washed with ethanol and water, and dried in an oven at 60 °C overnight under vacuum. The PNs were carbonized in a quartz tube at 800 °C for 2 h under a nitrogen atmosphere to obtain sample CNs. CNs were further mixed with powdered solid KOH (98%, Aldrich) at a mass ratio of 1:4 for chemical activation. The mixture was heated to 900 °C with a heating rate of 5 °C/min under a flow of nitrogen and retained for 2 h. The solid was finally washed with diluted HCl solution and copious water to completely remove metal species and dried at 120 °C for 4 h to obtain sample PCNs.

Pt catalysts supported on PNs, CNs, and PCNs were synthesized by the ethylene glycol (EG) reduction method.[36,37] Briefly, 50 mg of support nanospheres was mixed with 50 mL of EG (99.8%, Aldrich) under ultrasonic treatment for 30 min to obtain a liquid suspension. Then 1.68 mL of H_2PtCl_6 (38% Pt, Aldrich) solution (20 mg/mL Pt) was slowly dropped into the suspension, followed by stirring for 30 min and adjusting the pH to 11.0 using 1 M NaOH in E-G solution. The mixture was refluxed in a flask using a Milestone MicroSYNTH programmable microwave system (1000W, 2.45 GHz) for 3 min in the nitrogen atmosphere while stirring. The resulting suspension of Pt catalyst was centrifuged, washed with ethanol and deionized water, and dried at 80 °C in a vacuum oven overnight. The prepared Pt catalyst supported on PCNs, CNs, and PNs was assigned as Pt/PCN, Pt/CN, and Pt/PN, respectively.

2.2. Characterization. The N_2 adsorption isotherms of the samples were investigated using an ASAP2020 volumetric

(16) Ma, Y.; Jiang, S.; Jian, G.; Tao, H.; Yu, L.; Wang, X.; Wang, X.; Zhu, J.; Hu, Z.; Chen, Y. *Energy Environ. Sci* **2009**, *2*, 224–229.
(17) Kim, M.; Hwang, S.; Yu, J.-S. *J. Mater. Chem.* **2007**, *17*, 1656–1659.
(18) Di Noto, V.; Negro, E.; Gliubizzi, R.; Lavina, S.; Pace, G.; Gross, S.; Maccato, C. *Adv. Funct. Mater.* **2007**, *17*, 3626–3638.
(19) Yue, B.; Ma, Y.; Tao, H.; Yu, L.; Jian, G.; Wang, X.; Wang, X.; Lu, Y.; Hu, Z. *J. Mater. Chem.* **2008**, *18*, 1747–1750.
(20) Sun, C.-L.; Chen, L.-C.; Su, M.-C.; Hong, L.-S.; Chyan, O.; Hsu, C.-Y.; Chen, K.-H.; Chang, T.-F.; Chang, L. *Chem. Mater.* **2005**, *17*, 3749–3753.
(21) Lei, Z.; An, L.; Dang, L.; Zhao, M.; Shi, J.; Bai, S.; Cao, Y. *Microporous Mesoporous Mater.* **2009**, *119*, 30–38.
(22) Liu, H.; Shi, Z.; Zhang, J.; Zhang, L.; Zhang, J. *J. Mater. Chem.* **2009**, *19*, 468–470.
(23) Yuasa, M.; Yamaguchi, A.; Itsuki, H.; Tanaka, K.; Yamamoto, M.; Oyaizu, K. *Chem. Mater.* **2005**, *17*, 4278–4281.
(24) Lefevre, M.; Proietti, E.; Jaouen, F.; Dodelet, J.-P. *Science* **2009**, *324*, 71–74.
(25) Su, F.; Zhou, Z.; Guo, W.; Liu, J.; Tian, X. N.; Zhao. X. S. In *Chem. Phys. Carbon*; Radovic, L. R., Ed.; Marcel Dekker: New York, 2008; Vol. *30*, pp 63−128.
(26) Stein, A.; Wang, Z.; Fierke, M. A. *Adv. Mater.* **2009**, *21*, 265–293.
(27) Lei, Z.; Zhao, M.; Dang, L.; An, L.; Lu, M.; Lo, A.-Y.; Yu, N.; Liu, S.-B. *J. Mater. Chem.* **2009**, *19*, 5985–5995.
(28) Choi, B.; Yoon, H.; Park, I.-S.; Jang, J.; Sung, Y.-E. *Carbon* **2007**, *45*, 2496–2501.
(29) Sidik, R. A.; Anderson, A. B.; Subramanian, N. P.; Kumaraguru, S. P.; Popov, B. N. *J. Phys. Chem. B* **2006**, *110*, 1787–1793.
(30) Ikeda, T.; Boero, M.; Huang, S.-F.; Terakura, K.; Oshima, M.; Ozaki, J.-i. *J. Phys. Chem. C* **2008**, *112*, 14706–14709.
(31) Maldonado, S.; Stevenson, K. J. *J. Phys. Chem. B* **2005**, *109*, 4707–4716.
(32) Gong, K.; Du, F.; Xia, Z.; Durstock, M.; Dai, L. *Science* **2009**, *323*, 760–764.
(33) Matter, P. H.; Wang, E.; Arias, M.; Biddinger, E. J.; Ozkan, U. S. *J. Phys. Chem. B* **2006**, *110*, 18374–18384.
(34) Xie, F.; Tian, Z.; Meng, H.; Shen, P. K. *J. Power Sources* **2005**, *141*, 211–215.
(35) Wang, Y.; Su, F.; Wood, C. D.; Lee, J. Y.; Zhao, X. S. *Ind. Eng. Chem. Res.* **2008**, *47*, 2294–2300.
(36) Tian, Z. Q.; Jiang, S. P.; Liang, Y. M.; Shen, P. K. *J. Phys. Chem. B* **2006**, *110*, 5343–5350.
(37) Poh, C. K.; Lim, S. H.; Pan, H.; Lin, J.; Lee, J. Y. *J. Power Sources* **2008**, *176*, 70–75.

adsorption analyzer (Micromeritics, U.S.A.). The X-ray diffraction (XRD) patterns were collected on a Bruker D8 diffractometer. Thermogravimetric analysis (TGA) was conducted on a thermogravimetric analyzer TGA Q500 (Thermal Analysis Instruments, U.S.A.). The microscopic features of the samples were observed with a field-emission scanning electron microscope (SEM) (JSM-6700F, JEOL Japan) and field-emission transmission electron microscope (TEM) (Tecnai G^2 TF20 S-twin, FEI Company). Element content was analyzed with energy dispersive X-ray (EDX) spectroscopy at 15 kV with SEM. The surface chemical composition of the samples was determined by X-ray photoelectron spectroscopy (XPS) on a VG ESCALAB 250 spectrometer (Thermo Electron, U.K.), using a nonmonochromatized Al Kα X-ray source (1486 eV). The electrochemical performance of Pt catalysts was measured by cyclic voltammetry (CV) at room temperature in a three-electrode cell using Autolab PGSTAT302 electrochemical test system (Eco Chemie, The Netherlands). The details of the characterization techniques can be found in Supporting Information.

3. Results and Discussion

3.1. Characterization of Supports. Figure 1 shows the N_2 adsorption−desorption isotherms and pore size distribution (PSD) of support sample PCNs. It can be seen that the adsorption isotherm of PCNs in Figure 1a is of type I according to the IUPAC classification, indicative of microporous material. The remarkable nitrogen uptake above the relative pressure of 0.80 is due to the capillary condensation of nitrogen in interparticulate porosity that exists among agglomerate nanospheres forming a mesoporous texture. The inset in Figure 1a shows the PSD of PCNs derived from the density functional theory (DFT) method. The pore size of PCNs is centered at around 1.1 nm. The surface area of PCNs is 1010 m^2/g, about 10-fold higher than that of CNs (110 m^2/g, its isotherm is not shown here), indicating the dense structure of nonporous CNs. The surface area of PNs is 50 m^2/g (its isotherm is not shown here). In addition, our experiments demonstrated that direct chemical activation of PN could not produce PCNs, possibly due to the gasification of polypyrrole in the presence of KOH at the high temperature.

Figure 2 shows the SEM images of support samples PNs, CNs, and PCNs, together with TEM images of PCNS. It is seen that PNs in Figure 2a possess an overall monodisperse particle distribution, and their particle size is in the range of 100−140 nm in the diameter shown in Figure 2b. The EDX spectrum of PNs (not shown here) indicates the presence of C (70 wt %), N (19 wt %), O (8 wt %), Fe (2 wt %), and Cl (1 wt %). The atomic ratio of N/C is ∼0.23, consistent with that of the polypyrrole unit ($-C_4NH_2-$) (N/C = 0.25). Figure 2c shows the image of CNs, which are relatively smaller than their parent PNs due to the shrinkage during carbonization process. The rough surface of CNs may stem from the heterogeneous shrinkage. The mass content of C, N, O, and Fe derived from EDX analysis for sample CNs (not shown here) is 81 wt %, 10 wt %, 6 wt %, and 3 wt %, respectively, and no signal from Cl was detected. The N

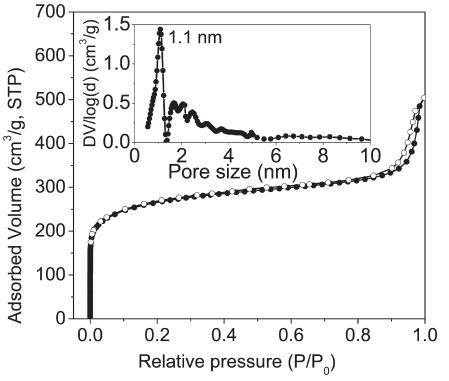

Figure 1. Nitrogen adsorption/desorption isotherms of PCNs, together with its PSD curve (inset).

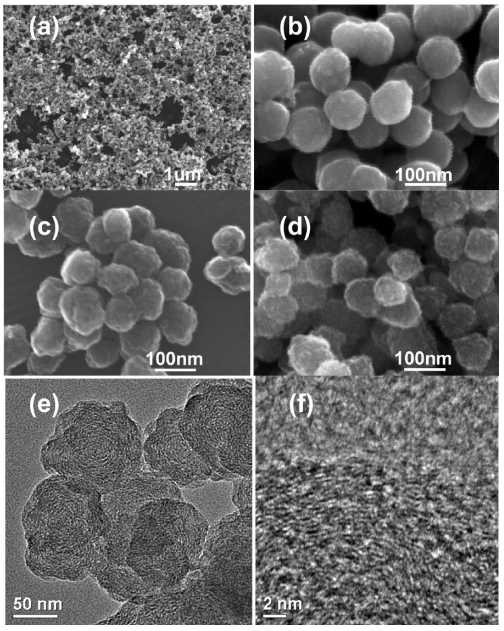

Figure 2. SEM images of catalyst supports PNs (a, b), CNs (c), and PCNs (d) and TEM images of PCNs (e, f).

content here is comparable to that of carbon nanofibers converted from polypyrrole.[16] The atomic ratio of N/C is approximate 0.11, almost half of that of the PNs, suggesting that the carbonization process would reduce the concentration of N species more quickly relative to C because the denitrogenation, dehydrogenation, and aromatization occurred. Figure 2d exhibits the morphology of PCNs, whose surface looks much coarser than CNs. This may result from the etching of the carbon matrix by chemical activating agent. C (88 wt %), N (4 wt %), O (6 wt %), and K (0.5%) in PCNs were found using EDX except for Fe. The atomic ratio of N/C is ∼0.04, much less than that of CNs. This may be because some N species within CNs are more active during chemical activation and readily gasified. TG curves of PCNs, CNs, and PNs (Figure S1a, Supporting Information) indicate that the residual weight for PCNs is negligible, but for CNs and PNs is ∼3.4 wt % and ∼2.2 wt %, respectively. The residue may be ascribed to the iron oxides, whose particles size is too small to be detected by XRD shown in Figure S1b (Supporting Information). Since the size of the PNs

can be easily tuned by controlling the feed amount of pyrrole monomer during the polymerization,[35] the particle size of PCNs can be tailored accordingly. TEM images of PNs and CNs can be found in Figure S2 (Supporting Information). The TEM image of the PCNs in Figure 2e clearly shows the microporous structure of PCNs with more exposed graphene edges as well as defects. PCNs also have much less dense molecular structure and indistinctly discrete graphene layers as shown in Figure 3f when compared to the image of CNs in Figure S2d (Supporting Information). These findings are consistent with the XRD analysis in Figure S1b (Supporting Information), in which XRD patterns of both carbon supports show a turbostratic structure with a large curvature of the graphene layers while the intensity of the (002) peak for PCNs is much less than that for CNs, suggesting a much lower graphitic crystallinity and more defects of the sample PCNs. It has been known that the chemical activation using KOH is a well established method to generate highly microporous structures for various carbonaceous materials.[38−40] At a high temperature, the alkali species is reduced to metal by the carbon species, and thus the carbon framework is etched to create a large number of micropores due to the oxidation of carbon into carbonate ion. The subsequent removal of the alkali metal species by washing with acid solution may generate additional micropores. Because at the activation temperature of 900 °C much higher than the melting point of KOH (~400 °C), KOH would be present as a liquid and is allowed facile diffusion within the carbon framework. Therefore, activation reaction homogeneously occurred between the activating agent KOH, and the carbon matrix generated a uniform micropore distribution within PCNS in Figure 2e. It should be mentioned that the chemical activation using KOH could introduce much oxygen functional groups and graphene layer defects on the surface of PCNs, which are significant for deposition and immobilization of Pt nanoparticles,[41] together with formation of strong interfacial interaction between Pt and carbon surface.[42−45]

3.2. Characterization of Pt Catalysts. The XRD patterns of Pt/PCN, Pt/CN, Pt/PN, and commercial E-TEK catalysts are shown in Figure 3a. The diffraction peaks at 2θ values of about 39.8°, 46.3°, 67.6°, and 81.5° are ascribed to the facets (111), (200), (220), and (311), characteristic of face-centered cubic (fcc) crystalline Pt (JCPDS, Card No. 04-0802), suggesting that Pt species were reduced to the metallic state by EG. The average size of the Pt nanoparticles was calculated from the Pt(220) peak using the Debye−Scherrer equation to be ~3.3, 4.0, 4.4, and 4.5 nm for Pt/PCN, Pt/CN, Pt/PN, and E-TEK, respectively. Figure 3b shows the TG curves of Pt/PCN, Pt/CN, Pt/PN, and E-TEK catalysts. It is seen that the weight loss of Pt/PN, Pt/CN, and Pt/PCN takes place in the temperature ranges 200−270, 270−350, and 310−380 °C, respectively, obviously lower than that of their supports shown in Figure S1a (Supporting Information). This is because the introduction of Pt metal nanoparticles led to the catalytic oxidation of support matrix in air. The temperature range for main weight loss of E-TEK is 350−430 °C, much higher than that of Pt/PCN possibly due to the higher surface area of PCNs than that of E-TEK support (~200 m^2/g), which may allow more graphene defects exposed for oxidation. In addition, it has been found that the N-doped graphene layer has apparently higher chemical reactivity toward oxygen than the undoped one due to more edge-active sites resulting from the introduction of N species,[31] leading to lower oxidation temperature. The weight loss for these samples below 200 °C should result from the desorption of water vapor and/or residual EG. Thus, the Pt metal content in the catalysts can be obtained from their TG curves after subtracting the weight of adsorbed water and residue. Setting the weight of the anhydrous material to 100 wt %, the contents of Pt in Pt/PCN, Pt/CN, Pt/PN, and E-TEK are 40.3, 36.4, 37.2, and 40.7 wt %, respectively.

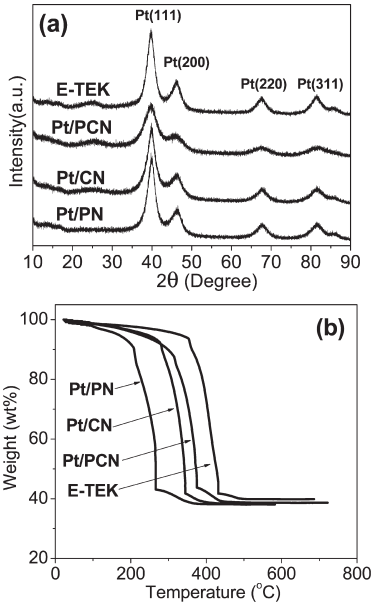

Figure 3. XRD patterns (a) and TG curves (b) of Pt/PCN, Pt/CN, Pt/PN, and E-TEK catalysts.

Figure 4 shows the TEM images of samples Pt/PN, Pt/CN, and Pt/PCN, as well as commercial E-TEK catalyst. The images of Pt/PN catalyst in Figure 4a,b show that Pt nanoparticles densely covered the surface of PNs possibly due to their much lower surface area, and Pt particle size is estimated to be ~5 nm. Figure 4c,d presents the images of Pt/CN catalyst, in which Pt nanoparticles were homogeneously dispersed on the surface of CNs and their size is ranged from 4 to 5 nm. In Figure 4e,f for Pt/PCN catalyst, it is clearly seen that Pt nanoparticles with a size of less

(38) Cheng, F.; Liang, J.; Zhao, J.; Tao, Z.; Chen, J. *Chem. Mater.* **2008**, *20*, 1889–1895.
(39) Jaroniec, M.; Choma, J.; Gorka, J.; Zawislak, A. *Chem. Mater.* **2008**, *20*, 1069–1075.
(40) Wang, J. N.; Zhang, L.; Niu, J. J.; Yu, F.; Sheng, Z. M.; Zhao, Y. Z.; Chang, H.; Pak, C. *Chem. Mater.* **2007**, *19*, 453–459.
(41) Chen, J.; Wang, M.; Liu, B.; Fan, Z.; Cui, K.; Kuang, Y. *J. Phys. Chem. B* **2006**, *110*, 11775–11779.
(42) Yang, D. Q.; Zhang, G. X.; Sacher, E.; Jose-Yacaman, M.; Elizondo, N. *J. Phys. Chem. B* **2006**, *110*, 8348–8356.
(43) Yang, D.-Q.; Sacher, E. *Chem. Mater.* **2006**, *18*, 1811–1816.
(44) Zhang, G.; Yang, D.; Sacher, E. *J. Phys. Chem. C* **2006**, *111*, 565–570.
(45) Yang, D. Q.; Sacher, E. *J. Phys. Chem. C* **2008**, *112*, 4075–4082.

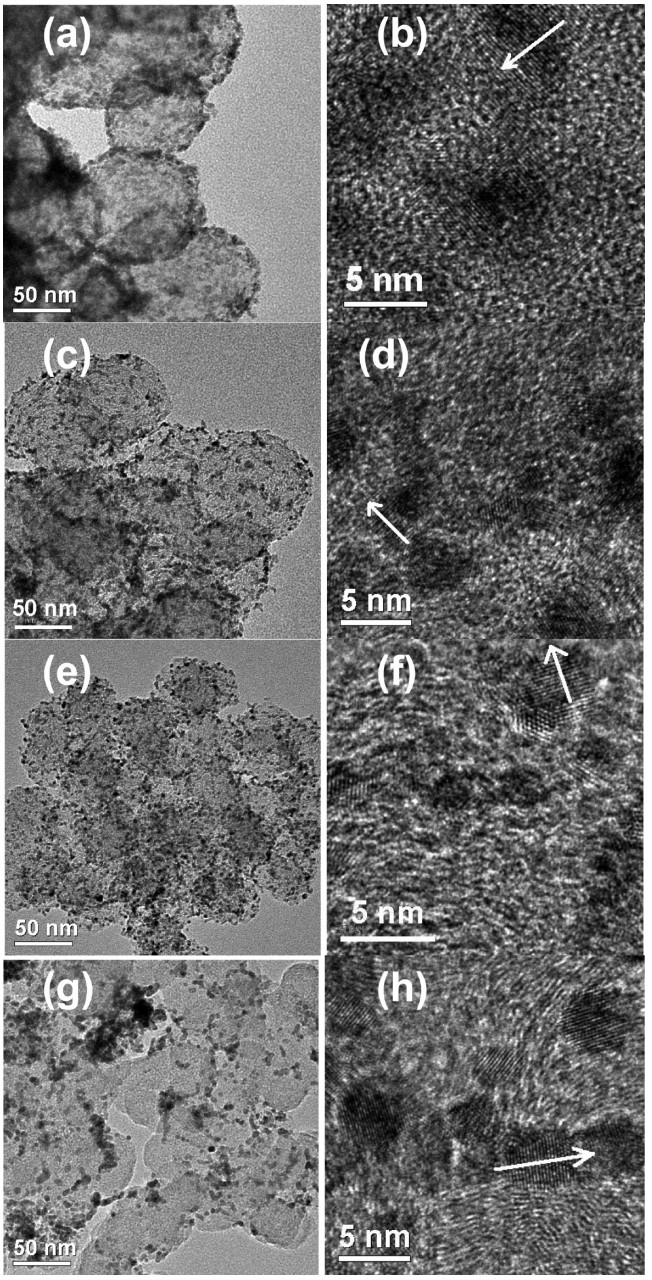

Figure 4. TEM images of Pt catalysts: (a, b) Pt/PN; (c, d) Pt/CN; (e, f) Pt/PCN; (g, h) E-TEK.

than 4.0 nm are homogeneously deposited on the surface of PCNs with the high dispersion. However, some aggregated Pt nanoparticles can be found in Figure 4g,h for E-TEK catalyst, and the Pt particle size is ~5 nm. The lattice distance as marked with the white arrows in Figure 4b,d,f, h is around 0.23 nm, in agreement with the interplanar distances of d_{111} in Pt crystal. Studies have proven that the presence of N species as localized defects facilitates the high dispersion and immobilization of Pt particles on the carbon supports and makes the carbon surface chemically active for the enhanced interaction between Pt and the supports.[5] For instance, Yue et al. found that Pt nanoparticles were homogeneously dispersed on the N-doped CNTs compared with pristine ones.[19] Here, it is believed that for all three synthesized catalysts, the N-participation in the connection of Pt species with the support[19] may

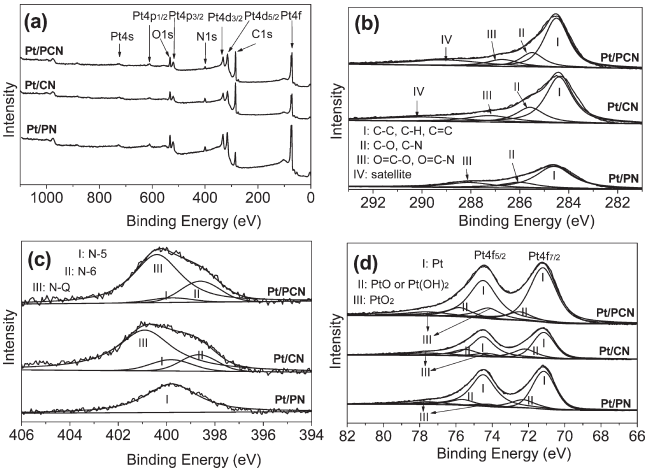

Figure 5. XPS spectra of Pt/PN, Pt/CN, and Pt/PCN catalysts: (a) wide scan, (b) C 1s, (c) N 1s, and (d) Pt 4f.

contribute to the high dispersion of Pt particles. In particular, for support PCNs, the creation of the developed pore structure, abundant functional sites (N- and O-species), and many defects derived from chemical activation process may form a strong interaction between Pt nanoparticles and carbon surface, responsible for the efficient deposition of Pt nanoparticles and avoidance of Pt particle coalescence.[42,43,45,46]

The XPS survey spectra of samples Pt/PN, Pt/CN, and Pt/PCN are depicted in Figure 5. The presence of C, N, O, and Pt elements can be clearly seen in the wide spectra for all catalysts in Figure 5a. The signal from the Fe element may be too weak or undetectable on the support surface to be found in these spectra similar to the XRD analysis in Figure S1b (Supporting Information). It is also clearly seen that the ratio of the area of the N 1s peak at a binding energy (BE) of around 400 eV over the area of C 1s peak at about 284.5 eV roughly goes as the sequence of Pt/PNs > Pt/CNs > Pt/PCN, in accordance with the above EDX analysis of supports.

Figure 5b shows the C 1s spectrum of three samples, fitted into four individual component peaks labeled with I, II, III, and IV, representing graphitic carbons with C═C, C—C, and C—H at a BE of 284.5 eV, carbons with C—O and/or C—N at around 285.7 eV, carbons O═C—O and/or O═C—N at around 287.0 eV, and a satellite signal due to $\pi-\pi^*$ transitions in aromatic rings at 289.4 eV, respectively.[47,48] Sacher and his coworkers demonstrated that the increase of full widths at half-maxima (fwhm) of peak I in the C 1s spectrum is closely related to the introduction of more defects and O species on the surface of treated highly oriented pyrolytic graphites (HOPGs, model carbon materials).[42,44] Here, the fwhm of peak I for PCNs (1.29 eV) is greater than for CNs (1.09 eV), presumably suggesting the more defects and/or O species on PCNs derived from the chemical

(46) Endo, M.; Kim, Y. A.; Ezaka, M.; Osada, K.; Yanagisawa, T.; Hayashi, T.; Terrones, M.; Dresselhaus, M. S. *Nano Lett.* **2003**, *3*, 723–726.
(47) Su, F.; Zhao, X. S.; Lv, L.; Zhou, Z. *Carbon* **2004**, *42*, 2821–2831.
(48) Ababou-Girard, S.; Sabbah, H.; Fabre, B.; Zellama, K.; Solal, F.; Godet, C. *J. Phys. Chem. C* **2007**, *111*, 3099–3108.

activation, in accordance with the observation of TEM (Figure 2e,f) and XRD analysis (Figure S1b, Supporting Information).

N 1s spectra of all samples are shown in Figure 5c. Using the integrated peak area ratio of the individual N 1s and C 1s peaks corrected by the atomic sensitivity factors, the N/C surface atomic ratio was calculated to be 0.19 for Pt/PN, 0.10 for Pt/CN, and 0.05 for Pt/PCN. These values are in good agreement with the results of above EDX analysis. The N/C ratio of PCNs is comparable to that of vertically aligned N-doped CNTs derived from polypyrrole (0.04−0.06),[32] but as a result, PCNs obtained here have a much higher surface area. The chemical activation to create PCNs from CNs resulted in a lower N content. The N 1s spectrum of materials shown in Figure 5c is fitted by three component peaks labeled with I, II, and III, which is ascribed to N-5, N-6, and N-Q, respectively.[49−52] N-5 represents pyrrolic-N in a five membered ring and/or pyridonic-N that is pyridinic-N in association with phenolic or carbonyl group on the neighbor carbon atom of the ring (sp^2 hybridization to C[53]). N-6 is pyridinic-N, that is, N bonded to two C atoms in six-membered rings at the edge of graphene layer (sp hybridization to C[53]). N-Q is quaternary-N, that is, N bonded to three C atoms in central or valley position of graphene layer. For the Pt/PN catalyst, there is only one peak observed at 399.8 eV (N-5), corresponding to N atoms within the pentagonal pyrrole ring of the polypyrrole. For Pt/CN, three peaks, N-5 (399.8 eV), N-6 (398.7 eV), and N-Q (401.0 eV) were observed. For Pt/PCN, it can be seen that N-5, N-6, and N-Q were located at 399.8, 398.7, and 400.5 eV respectively, and the proportion of N-5 is obviously shorter than that of CNs. The low shift of N-Q bending energy (−0.5 eV) for PCNs compared with CNs may be related to the chemical activation, which partially destroys the N-containing graphene structure. These results indicate that N atoms within the pentagonal ring of polypyrrole chemical structure (N-5) in PNs were converted to two types of N atoms (N-Q and N-6) in CNs and PCNs after heat treatment. The content of N-Q for both supports CNs and PCNs is seen to be much more than that of N-5 and N-6 content, suggesting that a majority of nitrogen atoms are located inside graphene layers and others are at the periphery of graphene layers. Although it is known that N species are responsible for the enhanced electrochemical performance, exact species, either N-Q[29,30] or N-6 (N-5),[54,55] is still unclear. Our results may infer that the N species at the edges of graphene layers in CNs and PCNs (N-6 and N-5) and N atoms within the pentagonal pyrrole ring of the PNs (N-5) may provide the main initial nucleation sites for the deposition of small Pt nanoparticles[54] and also active sites for Pt immobilization avoiding surface Pt diffusion and coalescence even at the high Pt loading.[16,19] This may be similar to the sulfur species introduced on the carbon surface, which has been demonstrated to lead to the Pt−S bonds or strong Pt−support interaction resulting in a very high loading, dispersion, and stability of Pt nanoparticles.[56−59] On the other hand, the N atom substitutes (N−Q) within graphene layers for CNs and PCNs could enhance the electric conductivity of carbon materials as indicated by our simulation[60] and confirmed by below impedance analysis.

Figure 5d presents the Pt 4f spectra of obtained catalysts, which can be deconvoluted into three pairs of doublets labeled with I, II, and III. The most intense doublet with BE of 71.2 eV (Pt $4f_{7/2}$) and 74.5 eV (Pt $4f_{5/2}$) was attributed to metallic Pt, but the peaks at around 72.2 and 75.5 eV could be assigned to the Pt^{2+} chemical state as in either PtO or $Pt(OH)_2$.[61] The third pair of peaks found at around 74.2 and 77.5 eV is most likely ascribed to Pt^{4+} species on the surface such as PtO_2.[62,63] These Pt oxide species may be due to oxygen chemisorption at step and kink sites present on the Pt surface.[64] The integration of peak areas indicates that most Pt species exist as metallic Pt for all catalysts. Pt nanoparticles on the three supports obtained seem very similar in the chemistry state based on the XPS analysis. It has been known that on the carbon supports, the decrease of Pt particle size could bring about the shift of the core-level Pt 4f spectrum to the high binding energy and the increase of its fwhm.[42,44,45] In our case, we hardly observe the clear shift of the Pt 4f peak position possibly due to the effect of the support chemistry, which may veil the peak shift. However, the fwhm of the Pt $4f_{7/2}$ (peak I at ~71.2 eV) for Pt/PCN, Pt/CN, and Pt/PN is ~1.66, 1.55, and 1.47, indicating the particle size goes as the order Pt/PCN < Pt/CN < Pt/PN, in good agreement with the XRD analysis in Figure 3a.

3.3. Electrochemical Performance of Pt Electrocatalysts. The electrochemical active surface areas of different catalysts were determined by CV measurement performed in 0.5 M H_2SO_4 aqueous solution as shown in Figure 6a. It can be seen that well-defined CV curves were obtained for three carbon-supported catalysts, Pt/PCN, Pt/CN, and E-TEK. In contrast, the CV curve for the

(49) Pels, J. R.; Kapteijn, F.; Moulijn, J. A.; Zhu, Q.; Thomas, K. M. *Carbon* **1995**, *33*, 1641–1653.
(50) Kapteijn, F.; Moulijn, J. A.; Matzner, S.; Boehm, H. P. *Carbon* **1999**, *37*, 1143–1150.
(51) Hulicova-Jurcakova, D.; Seredych, M.; Lu, G. Q.; Bandosz, T. J. *Adv. Funct. Mater.* **2009**, *19*, 438–447.
(52) Ania, C. O.; Khomenko, V.; Raymundo-Piñero, E.; Parra, J. B.; Béguin, F. *Adv. Funct. Mater.* **2007**, *17*, 1828–1836.
(53) Yang, D. Q.; Sacher, E. *Surf. Sci.* **2003**, *531*, 185–198.
(54) Roy, S. C.; Harding, A. W.; Russell, A. E.; Thomas, K. M. *J. Electrochem. Soc.* **1997**, *144*, 2323–2328.
(55) Ozaki, J.-i.; Tanifuji, S.-i.; Kimura, N.; Furuichi, A.; Oya, A. *Carbon* **2006**, *44*, 1324–1326.
(56) Yang, D. Q.; Hennequin, B.; Sacher, E. *Chem. Mater.* **2006**, *18*, 5033–5038.
(57) Lee, H. I.; Joo, S. H.; Kim, J. H.; You, D. J.; Kim, J. M.; Park, J.-N.; Chang, H.; Pak, C. J. Mater. Chem. **2009**, DOI: 10.1039/b907514c
(58) Kim, Y.-T.; Ohshima, K.; Higashimine, K.; Uruga, T.; Takata, M.; Suematsu, H.; Mitani, T. *Angew. Chem., Int. Ed.* **2006**, *45*, 407–411.
(59) Kim, Y.-T.; Mitani, T. *J. Catal.* **2006**, *238*, 394–401.
(60) Lim, S. H.; Li, R.; Ji, W.; Lin, J. *Phys. Rev. B* **2007**, *76*, 195406.
(61) Liu, Z.; Lin, X.; Lee, J. Y.; Zhang, W.; Han, M.; Gan, L. M. *Langmuir* **2002**, *18*, 4054–4060.
(62) Liu, Z.; Lee, J. Y.; Chen, W.; Han, M.; Gan, L. M. *Langmuir* **2004**, *20*, 181–187.
(63) Liang, Y.; Zhang, H.; Zhong, H.; Zhu, X.; Tian, Z.; Xu, D.; Yi, B. *J. Catal.* **2006**, *238*, 468–476.
(64) Aricò, A. S.; Shukla, A. K.; Kim, H.; Park, S.; Min, M.; Antonucci, V. *Appl. Surf. Sci.* **2001**, *172*, 33–40.

polymer-supported Pt/PN catalyst shows a flat profile, indicating it almost has no detectable activity toward hydrogen adsorption/desorption. In general, the cathodic and anodic peaks appearing between −0.2 V and 0.10 V originate from the adsorption and desorption of atomic hydrogen on the Pt surface in acidic media, respectively. Thus, from the area of H-adsorption,[36] electrochemical active area (EAA) of Pt/PCN, Pt/CN, and E-TEK catalysts was calculated to be 246, 183, and 191 cm^2/mg, respectively. High EAA of Pt/PCN may originate from the more exposed Pt atoms on the finer Pt nanoparticles and would be responsible for the good electrochemical catalytic performance.

The electrocatalytic activities of the catalysts toward MOR are shown in Figure 6b. The methanol oxidation activity is reflected by the magnitude of the anodic peak current in the forward scan while the peak in the reverse scan is due to the reactivation of Pt associated with the removal of the residual carbon species.[62] In the forward scan, although a similar onset potential at which the methanol oxidation initiates is observed for Pt/PCN, Pt/CN, and E-TEK, their methanol oxidation peaks are located at 0.65, 0.70, and 0.66 V, and their mass catalytic activities (peak current density, which have been normalized to the Pt loading) are 343, 297, and 300 mA/mg, respectively. Pt/PCN shows the highest mass activity and the lowest oxidation potential, which are desired for MOR. The Pt/CN catalyst has a comparable mass activity to that of commercial E-TEK catalyst but with a higher oxidation potential that is undesired. It was also found that after 500 cycles in Figure S3 (Supporting Information), activity of Pt/PCN is still the highest even if substantially reduced to ~65% of its initial value, indicating its good stability for MOR comparable to the E-TEK catalyst. In contrast, no clear peaks can be observed in the CV curve of Pt/PN in Figure 6b, implying catalyst Pt/PN is also catalytically inactive for MOR. However, the result for Pt/PN is against the previous work, in which for MOR, Pt nanoparticles supported on polypyrrole nanowires (a polymer support) showed a higher initial activity than on carbon nanofibers as well as carbon black XC-72,[16] and Pt catalyst supported on polypyrrole-coated polystyrene spheres (a polymer support) showed superior properties compared with the commercial E-TEK catalyst.[34] The reason is unclear and may be the difference in the conductivity of polypyrrole synthesized with different approaches.

Figure 6c shows typical ORR polarization curves of Pt catalysts obtained at room temperature in O_2-saturated 0.5 M H_2SO_4 using a rotating disk electrode (RDE) at 2000 rpm. It is further evident that, compared with three carbon-supported catalysts, Pt/PN still has a negligible activity for ORR. The polarization curves of all carbon-supported catalysts exhibit two distinguishable potential regions, well-defined diffusion limiting currents (0.0−0.3 V) followed by a mixed kinetic-diffusion control region in the potential window of 0.4−0.7 V with the onset potential of around 0.80 V. The limiting current for Pt/PCN, Pt/CN, and E-TEK is around 138, 119, and 101 mA/mg,

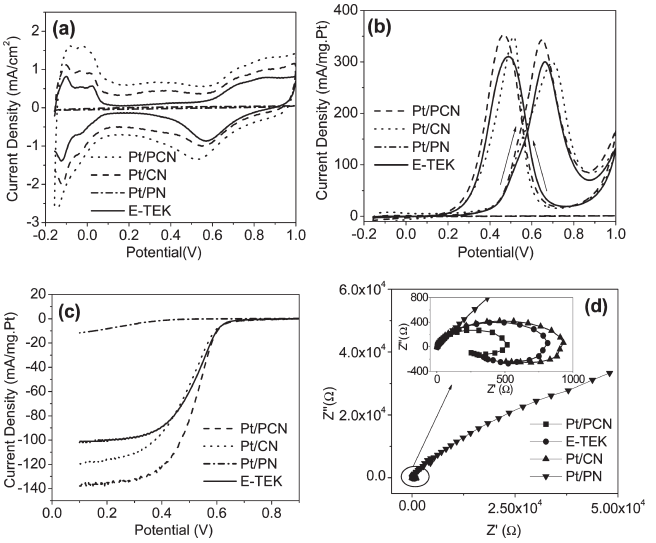

Figure 6. (a) CV curves of catalysts measured in the electrolytes of 0.5 M H_2SO_4 at a scan rate of 50 mV/s; (b) CV curves of catalysts measured in electrolytes of 0.5 M H_2SO_4 + 1.0 M CH_3OH at a scan rate of 50 mV/s; (c) ORR curves of Pt catalysts in electrolytes of 0.5 M H_2SO_4 saturated with O_2 at a rotation rate of 2000 rpm and scan rate of 5 mV/s; (d) EIC curves of catalysts in 0.5 M H_2SO_4 + 1.0 M CH_3OH solution at 0.4 V.

respectively. The half-wave potential of the Pt/PCN, E-TEK, and Pt/CN is 0.52, 0.52, and 0.49 V, respectively. The mass activity was derived in the mixed-controlled domain at 0.55 V[65] to be 45 mA/mg for Pt/PCN, 35 mA/mg for E-TEK, and 28 mA/mg for Pt/CN, following the order: Pt/PCN > E-TEK > Pt/CN. The results exhibit that Pt/PCN possesses a better performance than Pt/CN and E-TEK catalysts.

The electrochemical impedance spectroscopy (EIS) technique has been used to probe the interfacial processes and kinetics of electrode reactions in electrochemical systems. The measured impedance can be presented in the form of imaginary (Z'') vs real (Z') parts at various frequencies, namely, Nyquist plots (also Argand-type diagrams), which appear as a multitude of semicircles and/or lines allowing the electrochemical reaction rate, charge transfer resistance, double layer capacitance, and ohmic resistance to be compared. The methanol electrooxidation on different catalysts at different potentials shows different impedance patterns for DMFC.[66−69] The Nyquist plots of the four catalysts are shown in Figure 6d. It can be seen that compared with the three carbon-supported Pt catalysts, polymer-supported Pt/PN catalyst possesses a tremendous large arc, suggesting a very slow or negligible reaction rate of methanol oxidation and extremely large charge transfer resistance. This may be due to the low conductivity of polymer support PNs. The intercept of the curves with the real

(65) Ignaszak, A.; Ye, S.; Gyenge, E. *J. Phys. Chem. C* **2009**, *113*, 298–307.
(66) Hsing, I.-M.; Wang, X.; Leng, Y.-J. *J. Electrochem. Soc.* **2002**, *149*, A615–A621.
(67) Chakraborty, D.; Chorkendorff, I.; Johannessen, T. *J. Power Sources* **2006**, *162*, 1010–1022.
(68) Hsu, N.-Y.; Yen, S.-C.; Jeng, K.-T.; Chien, C.-C. *J. Power Sources* **2006**, *161*, 232–239.
(69) Wang, Z.-B.; Yin, G.-P.; Shao, Y.-Y.; Yang, B.-Q.; Shi, P.-F.; Feng, P.-X. *J. Power Sources* **2007**, *165*, 9–15.

axis (Z') in the high frequency range for all catalysts in Figure S4 (Supporting Information) also indicates that the PNs have more ohmic resistance than PCNs and CNs. It was reported that the nanostructured polypyrrole showed typical nonmetallic behavior with a conductivity of 7.3×10^{-3} S/cm,[70] which is much less than that of common carbon materials.[71] Ando et al.[72] found that the electric conductivity of polypyrrole-derived materials carbonized at 750 °C was increased by a factor of approximately 10^4 compared with initially pure polypyrrole. Therefore, the extremely low conductivity (or high resistance) of support PNs compared with carbon supports (PCNs, CNs, and carbon black) may make charge or electron transfer impossible in the electrodes resulting in the inactivity of Pt/PN catalyst for MOR and ORR. The inset of Figure 6d shows the enlarged impedance patterns of catalysts, in which a typical pseudoinductive behavior with a large arc at high frequency and a small arc in the fourth quadrant at low frequency was observed. The small diameter of arc for Pt/PCN at high frequency indicates the small charge transfer resistance for MOR. The smaller intersect of impedance with the real axis (Z') (designated as polarization resistance) at low frequency for Pt/PCN compared with Pt/CN and E-TEK suggests the faster overall MOR rate, namely, dehydrogenation of methanol molecules and oxidation of intermediate CO_{ads} species.[66−69] EIS observation is consistent with the results in Figure 6a−c, further confirming the enhanced electrocatalytic activity of Pt/PCN catalysts. Since the methanol electrooxidation at different potentials and temperatures also shows different impedance behaviors, more EIS measurement may be needed for detailed mechanism study.

Our present investigation is still insufficient to identify both the exact role of N species for formation of Pt nanoparticles and the inactivity of Pt deposited on PNs using EG method. However, microporous PCNs were successfully developed as an excellent electrochemical material for Pt electrocatalyst support: large external surface area/volume ratio helpful for the high dispersion of Pt nanoparticles, highly developed pore structure ready for reaction mass transport,[73,74] abundant functionalities (N and O) and defects for deposition, and interaction of Pt nanoparticles on supports. Importantly, both computations[29,30] and experiments[31−33] have demonstrated the promising applications of N-doped carbon materials as metal-free catalysts toward ORR. In addition, PCNs could be promising electrode materials in supercapacitors because of the presence of N species that can lead to large pseudocapacitance[75] and the developed pore structure that could facilitate the transportation of electrolyte ions.[76] Our previous work demonstrated the potential applications of CNs in Li-ion batteries[35] and PNs in catalysis.[77] The investigation of PCNs, CNs, and PNs as electrode materials for supercapacitors and metal-free catalysts is underway.

4. Conclusions

In summary, N-doped porous carbon nanospheres (PCNs) were prepared by chemical activation of nonporous carbon nanospheres (CNs) that were obtained via carbonizing polypyrrole nanospheres (PNs). It was found that, after chemical activation using KOH as an activating agent, PCNs with N-functional groups (pyridinic-type and graphite-type) possessed a microporous structure with a surface area of 1010 m^2/g and a particle size of less than 100 nm. The N/C atomic ratio obtained by XPS was reduced from 0.19 for PNs to 0.10 for CNs and 0.05 for PCNs. The electrochemical properties of Pt/PCN, Pt/CN, and Pt/PN catalysts showed that Pt/PN catalyst is inactive toward methanol oxidation reaction (MOR) and oxygen reduction reaction (ORR) at room temperature due to the high intrinsic resistance of PNs. Compared to Pt/CN and commercial E-TEK catalyst (40 wt % Pt), Pt/PCN revealed an enhanced performance in ORR and MOR because of the high dispersion of small Pt nanoparticles on PCNs which possess a developed pore structure, high surface area, and N species. These nanosphere materials are expected to be applied as functional materials in energy conversion and storage and chemical catalysis.

Acknowledgment. We thank ICES of A*STAR and IPE of CAS for financial support and A.I. Cooper at the University of Liverpool for allowing to use ASAP2020.

Supporting Information Available: The details of the characterization techniques, TG curves and XRD patterns of samples PNs, CNs and PCNs, TEM images of PNs and CNs, CV curves of the catalysts measured for 500 cycles, and EIC curves of the catalysts at the high frequency (PDF). This material is available free of charge via the Internet at http://pubs.acs.org

(70) Zhang, X.; Zhang, J.; Song, W.; Liu, Z. *J. Phys. Chem. B* **2006**, *110*, 1158–1165.
(71) Celzard, A.; Marêché, J. F.; Payot, F.; Furdin, G. *Carbon* **2002**, *40*, 2801–2815.
(72) Ando, E.; Onodera, S.; Iino, M.; Ito, O. *Carbon* **2001**, *39*, 101–108.
(73) Su, F.; Zeng, J.; Bao, X.; Yu, Y.; Lee, J. Y.; Zhao, X. S. *Chem. Mater.* **2005**, *17*, 3960–3967.
(74) Lin, M. L.; Huang, C. C.; Lo, M. Y.; Mou, C. Y. *J. Phys. Chem. C* **2008**, *112*, 867–873.
(75) Hulicova, D.; Kodama, M.; Hatori, H. *Chem. Mater.* **2006**, *18*, 2318–2326.
(76) Largeot, C.; Portet, C.; Chmiola, J.; Taberna, P. L.; Gogotsi, Y.; Simon, P. *J. Am. Chem. Soc.* **2008**, *130*, 2730–2731.
(77) Tian, X.; Su, F.; Zhao, X. S. *Green Chem.* **2008**, *10*, 951–956.